ISBN: 978-3-95450-234-9 ISSN: 2673-5504 doi:10.18429/JACoW-SRF2023-TUPTB060

RECONSTRUCTION OF FIELD EMISSION PATTERN FOR PIP-II LB650 CAVITY

E. Del Core, M. Bertucci, A. Bosotti, A. T. Grimaldi, L. Monaco, C. Pagani[1],
R. Paparella, D. Sertore, INFN Milano - LASA, Segrate, Italy
[1] also at Università degli Studi di Milano, Segrate, Italy

Abstract

Field emission (FE) is a key limiting phenomenon in SRF cavities. An algorithm exploiting a self-consistent model of cavity FE has been developed. This method exploits experimental observables (such as Q value , X-ray endpoint, and dose rate) to reconstruct emitter position and size as well as the field enhancement factor. To demonstrate the model's self-consistency, the algorithm has been applied to the test results of a PIP-II LB650 prototype cavity. The results of the procedure are here described.

INTRODUCTION

One of the most limiting factor to the accelerating gradient in superconducting radio-frequency (SRF) cavities is Field Emission (FE). This phenomenon is associated with the surface electric field and refers to the emission of electrons from regions of high electric field on the cavity surface [1,2]. These emitted electrons, originating from the *emitters* sites, are accelerated by the RF field until they impact the cavity surface. As a result of this impact, X-ray radiation can be generated. The power deposited by the impacting electron depends both on the trajectory of the particle and on the intrinsic properties of the emitter. In SRF cavities, FE scales exponentially with the electric field and contributes to the consume of RF power. Consequently, it may correspond to an undesirable and unavoidable degradation of the Q-value, leading to an increase in cryogenic consumption [3].

Physical Description

In a metal, electrons are typically confined by a potential barrier that cannot be escaped in normal conditions. This gap between the Fermi level in the metal and the vacuum level, referred to as the metal work function and having a value of 4-5 eV, can be overcome when electron acquires energy through thermionic emission or photoemission phenomena. Under the influence of an applied electric field, the potential barrier assumes a triangular shape and its width diminishes as the field strength increases. Consequently, when the barrier becomes sufficiently thin, there exists a non negligible probability for electrons to tunnel it and escape from the surface [4] (see Fig. 1).

The tunnel probability and then the current I emitted by one site is described by the Fowler-Nordheim (FN) relation [5]:

$$I = S\frac{A_{FN}E^2\beta^2}{\phi}\exp\left(-\frac{B_{FN}\phi^{3/2}}{\beta E}\right), \qquad (1)$$

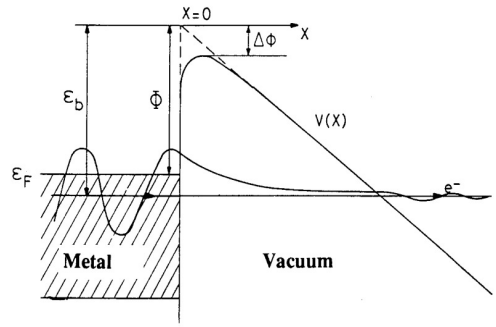

Figure 1: Potential barrier of metals with an applied E field to the surface [5].

where $A_{FN} = 1.54\times10^6$, $B_{FN} = 6.83\times10^3$, β is the field enhancement factor, ϕ is the work function eV and $E_s(t) = E_{s0}\sin(2\pi ft)$, measured in MV/m, is the instantaneous value of the surface electric field.

THEORETICAL APPROACH

Experimental Setup

What we currently use to analyze field emission in superconducting cavities, from a practical point of view, is:

- External radiation detectors: a portion of the impact electron energy is converted into X ray Bremsstrahlung radiation. The maximum X-ray energy (endpoint) corresponds to kinetic energy of the electrons at the impact point. To monitor the dose rate and partially simulate the power drained by electron dark current, a proportional counter[1] has been employed in the available setup. Additionally, a scintillator (NaI(Tl)) is utilized to capture the X-ray spectrum, enabling the evaluation of the endpoint, except in case of severe pile-up events determined by the poor shielding offered by the cryogenic structure (lead shielding brick are sometimes used (see Fig. 2).
- Inner diagnostic devices, such as electron pick-up probe and an array of photodiodes.
- Cavity Q drop measurement: it offers a means to evaluate the overall power of field emission if it is the dominant factor limiting the performance.

[1] Gas-filled (Xe) proportional counter. Measurement range from 100 nSv/h to 1 Sv/h; continuous acquisition every 1 s; energy rage from 45 keV to 1 MeV, so poor sensitivity for higher energies.

ISBN: 978-3-95450-234-9 ISSN: 2673-5504 doi:10.18429/JACoW-SRF2023-TUPTB060

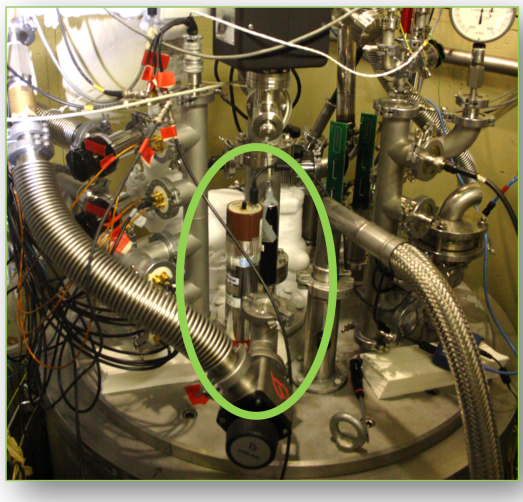

Figure 2: External radiation detectors placed on the cryostat cover.

Being Q_0 the quality factor without FE, l the accelerating length and R/Q the cavity geometric shunt impedance, the field-dependent effect of FE on the quality factor can be evaluated as:

$$\frac{1}{Q(E_{acc})} = \frac{1}{Q_0} + \frac{R}{Q}\frac{P_{FE}}{(E_{acc}l)^2}. \quad (2)$$

In this case the total dissipated power is given by P_d=P_c+P_{FE}, where P_c is the power dissipated in cavity walls.

How to Evaluate the REAL FE Impact

External detectors have a limited field of view, which means they can only observe a restricted portion of the emission pattern. Moreover, the emitted radiation undergoes several attenuation phenomena before reaching the detector active volume. As a limit case, if the electron impact energies are too low, FE may not be detected. As a result, it becomes challenging to determine the activated emitter positions "a priori". Inner detectors, such as photodiodes, can assist in reconstructing the emission pattern. Anyway, there is currently a lack of quantitative calibration for these sensors, although efforts are underway to address this limitation. Furthermore, field emission can be coupled with other phenomena, such as secondary emission (multipacting), parasitic mode excitation, thermal-induced quench in regions experiencing high impact current. These additional factors can further complicate the comprehensive modeling of cavity behavior.

Model of FE

The adopted approach begins with experimental investigation and subsequently incorporates a theoretical framework to ensure consistency between the model and the measurements. The objective of this endeavor is to utilize experimental observables, including *dose rate*, *energy endpoint*, and *Q-drop*, to establish a self-consistent model of FE within the cavity. This entails determining key parameters such as *emitter position*, *emitter size* and *field enhancement factor*.

From a computational perspective, the FishPact program [6], a 2D model for electron energies and tracking simulations, is employed as the starting point. To simulate pure field emission events, multipacting events have been neglected (impact number set to 1). This implies that the electron is absorbed upon its first impact with the cavity walls. There are pros and cons in the use of this solver despite of more advanced software such as CST: while this solver lacks advanced post-processing features and emission models, it offers significantly faster computational speed.

The field enhancement factor [7], denoted as β, takes into account the field emitter geometry. It depends on the emitter height, the radius of curvature of the apex and the shape of the emitter. The field enhancement factor can be computed by fitting the FN equation with the dose rate:

$$\log\frac{R}{E^2} = \log A - \frac{B}{\beta E}, \quad (3)$$

where A and B are two coefficients. The dose rate is expected to be proportional to the electron current:

$$R \propto \frac{1}{T}\int N(E)dE. \quad (4)$$

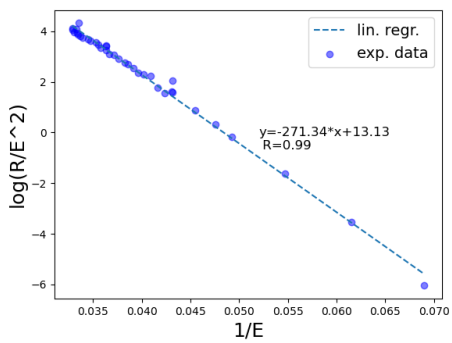

Figure 3: Field enhancement factor β fit.

As an example, Fig 3 shows the FN fit performed for exploiting the angular coefficient of the derived curve, the procedure was applied to the case of B61-EZ-002 PIP-II cavity. It resulted in an estimated value of β (see Fig. 3) of approximately 250-300.

Solver Steps

The solver utilizes the output files of FishPact, which contain information on electron trajectories and impact energies, to reconstruct the profile of field emission event based on the Fowler-Nordheim law. The objective is to obtain a probability distribution of the emission event, enabling an understanding of the likely trajectories and impact points along the cavity profile.

ISBN: 978-3-95450-234-9 ISSN: 2673-5504 doi:10.18429/JACoW-SRF2023-TUPTB060

This paragraph outlines the steps followed in the development of the solver. For each value of the accelerating field, the following procedures are carried out:

- Multiple emitter sites are tested along the cavity profile;
- The electron current is modeled according to the Fowler Nordheim emission law;
- Colliding electron trajectories are collected within a specific region on the cavity surface, considering the angle of view of the external detector. Each trajectory of interest is univocally determined by the emission phase φ_i. For each value of the collected trajectories, the impact energy $E(\varphi_i)$ and the number of emitted particles $N(\varphi_i)$ are evaluated;
- The simulated data are post-processed to obtain the overall impact electron energy spectrum as a function of E_{acc}.

Obviously the highest impact energy corresponds to maximum X-ray Bremsstrahlung Energy. These initial steps enable the first cross-check with experimental data, specifically with the X-ray energy spectrum σ(E).

Subsequently, by computing the power drained by electron dark current P_{FE}, which depends on the area of the emitter site, by summing up over the entire cavity surface as a function of E_{acc}, the Q_0 vs E_{acc} trend can be reconstructed.

$$P_{FE} = \frac{1}{T_{RF}} \sum_i N(\varphi_i) E(\varphi_i), \tag{5}$$

where E is the final impact energy [eV], T_{RF} is the RF period [s], $N(\varphi)$ is the number of emitted particles over a certain phase and φ is the emission phase [deg]. The second cross-check with experimental data is performed by comparing the simulated quality factor Q to the experimental one exploiting Eq. (2).

CASE STUDY PIP-II EZ-002 CAVITY

To validate the model, the prototype multicell B61-EZ-002 PIP-II cavity was selected as a case study. The results of the vertical test (VT) conducted at the LASA laboratory were utilized and are here presented and discussed.

During the first VT, as depicted in Fig. 4, some instances of multipacting with radiation were observed. Then, at an accelerating gradient field of 20.8 MV/m, a sudden increase in radiation which generated a testing instability. This behavior suggests the presence of a defect that altered its topology after being heated during high-field cavity operation.

Subsequently, the test was repeated, starting from low fields to avoid He-bath instabilities, and the same behavior as the first test was replicated until reaching 14 MV/m. At that point, there was a sudden rise in radiation and a corresponding drop of the Q_0 value. The cavity ultimately experienced quenching at 23 MV/m with Field Emission. Based on there results, it can be inferred that an irreversible activation of a field emitter likely occurred. Furthermore,

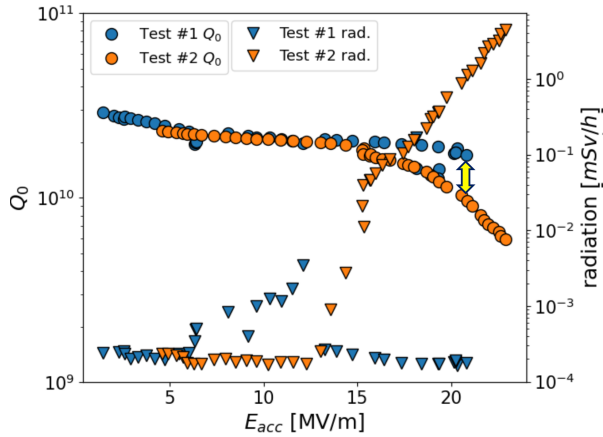

Figure 4: Q_0 vs E_{acc} graph for the 2 tests performed at LASA. The Q variation is assumed to be due to Field Emission, considering the same value of E_{acc}.

since the variation in the Q value was solely attributable to FE in this case, it served as an ideal test bench to assess the self-consistency of the model through the computation of P_{FE} (Eq. (2)).

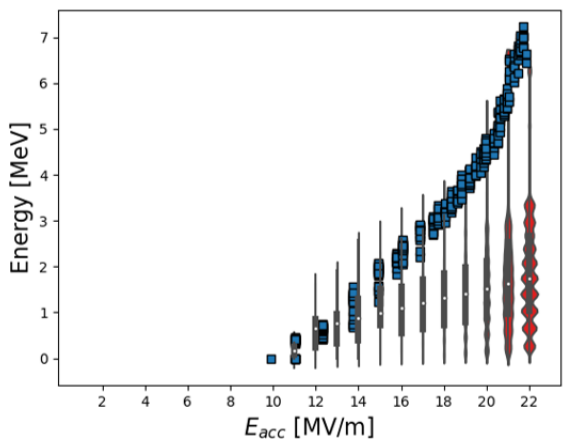

Figure 5: Computed density distribution (red violin plot) compared to scintillator data (blue squares).

Simulation Results

Numerous simulations were conducted using FishPact, varying the accelerating gradient, emitter site position, and its size. The first step involved calculating the value of E_{acc}/E_{peak} for all coordinates along the cavity profile, based on the SuperFish [8] output file for the specific cavity profile of interest. Subsequently, leveraging the FishPact output files, a script discretizes the Fowler-Nordheim law within a given range of E_{acc} and phase, and applies it to electron trajectories to obtain the probability distribution.

The reconstructed density distribution, depicted in Fig. 5 as the red violinplot[2], is compared to the x-ray endpoints

[2] Graphical representation of numeric data distributions are depicted using density curves, where the width of each curve corresponds to the frequency of data points in each region.

ISBN: 978-3-95450-234-9 ISSN: 2673-5504 doi:10.18429/JACoW-SRF2023-TUPTB060

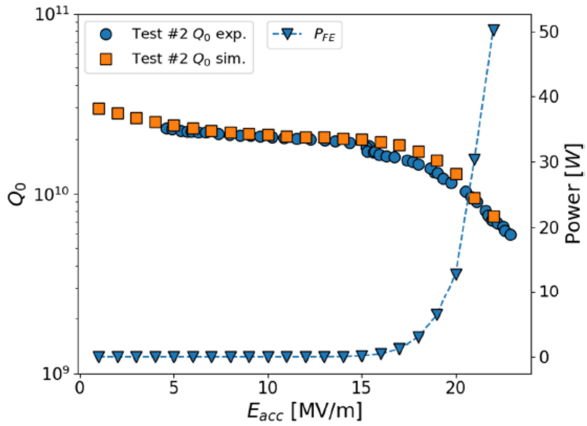

Figure 6: Q_0 vs E_{acc} reconstructed profile (orange squares) compared to experimental Q_0 vs E_{acc} (blue circles). Blue triangles show the P_{FE} computed values.

extracted from the scintillator energy spectra. It is worth noting that a good agreement between the computed and measured data is observed up to 20 MV/m. However, at higher fields, the detector[3] saturates, experiencing a severe count pile-up.

Figure 6 presents a comparison between the computed Q_0 (represented by orange squares) and the measured Q_0 (represented by blue circles). Once again, a good agreement between the two trends can be observed. This agreement indicates that a satisfactory solution has been found for estimating the position and size of the suspected emitter site.

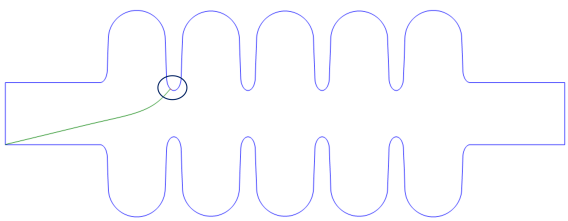

Figure 7: Estimated emitter site position.

The estimated characteristics for the emitter site, obtained from various simulations and yielding the best agreement between simulated and experimental data, are an *area* of 1.5×10^{-15} m^2 and a *position nearby iris 2* (see Fig. 7). A field enhancement factor of 300 has been used as obtained by fitting the dose rate vs E_{acc} data. Furthermore, a plot of the power due to field emission (represented by blue triangles) is included. Here, it is notable that power begins to rise at approximately 19 MV/m, and at 20 MV/m, it reaches 12 W. It is worth noting that the maximum cryogenic power that can be sustained for cavity CW operation is approximately 50 W.

[3] The detector used has a maximum count rate of 10^6 counts/sec, an energy range from a few keV to 10 MeV, and high sensitivity to radiation. Consequently, it is necessary to screen it with high Z material to mitigate pile-up effects.

CONCLUSION

In this study, we developed a model capable of reconstructing field emission behavior, based upon the already existing FishPact code. The program allows for the evaluation of various physical parameters corresponding to experimental observables, such as energy spectrum and total dissipated FE power, employing both analytical methods and dedicated software simulations. The self-consistency of the model was verified using the case of PIP-II cavity B61-EZ-002, which provided data with and without field emission. The impact energy distribution and field emission power were found to be consistent for each value of the accelerating gradient.

Several aspects remain open for further implementation to enhance the program comprehensiveness. Firstly, modeling the electron-to-photon count deconvolution is necessary to exploit also dose rate measurements. Additionally, the evaluation of pile-up statistics for detectors operating at high count rates should be addresses. Lastly, the convergence of the model when sampling with smaller phase steps needs to be studied to strike a balance between computational speed and model accuracy.

To enhance the quantitative aspect of our study, our future plans involve the development of a more complete model based on FLUKA. This advanced model is intended to provide an accurate description of the radiation-matter interaction process. Our objective is to develop a dedicated routine that integrates the Fowler-Nordheim law directly into the FLAIR interface. This integration will enable us to reconstruct the field emission process with improved precision. Currently, our focus lies on the implementation of the elliptical cavity geometry. However, this task presents challenges due to the boolean logic involved in the geometrical construction within FLUKA [9].

REFERENCES

[1] H. Padamsee, J, Knobloch, and T. Hays, "RF Superconductivity for Accelerators", in *Wiley series in beam physics and accelerator technology*, Cornell University, Ithaca, NY, USA, pp. 227–279.

[2] R. G. Forbes, J. H. B. Deane, A. Fischer, and M. S. Mousa, "Fowler-Nordheim Plot Analysis: a Progress Report", *Jordan J. Phys.*, vol. 8, 2015. doi:10.48550/arXiv.1504.06134

[3] J. Knobloch and H. Padamsee, "Explosive Field Emitter Processing in Superconducting RF Cavities", in *Proc. SRF'97*, Padova, Italy, Oct. 1997, paper SRF97D22, pp. 994–1016.

[4] T. Wang, C. Reece, and R. Sundelin, "Field emission study from Nb surface relevant to SRF cavities", in *Proc. PAC'03*, Portland, OR, USA, May 2003. doi:10.1109/PAC.2003.1289718

[5] B. Bonin, "Field Emission in RF cavities", DSM/DAPNIA, France, CEA-DAPNIA-SEA–96-03, 1996. https://cds.cern.ch/record/399571/files/p221.pdf

[6] E. Donoghue *et al.*, "Studies of Electron Activities in SNS-Type Superconducting RF Cavities", in *Proc. SRF'05*, Ithaca, NY, USA, Jul. 2005, paper TUP67, pp. 402–405.

ISBN: 978-3-95450-234-9 ISSN: 2673-5504 doi:10.18429/JACoW-SRF2023-TUPTB060

[7] D. Biswas, "A universal formula for the field enhancement factor", 2018. doi:10.48550/arXiv.1801.09990

[8] M. T. Menzel and H. K. Stokes, *User's Guide for the POISSON/SUPERFISH Group of Codes*, Los Alamos, 1987.

[9] M. Santana Leitner, "Studies of radiation fields of LCLS-II super conducting radio frequency cavities", *Int. J. Mod. Phys. Conf. Ser.*, vol. 44, 2016. doi:10.1142/S201019451660209X